Framework for Static and Dynamic Friction Identification for Industrial Manipulators

A framework for static and dynamic friction identification for industrial manipulators

Marina Indri, *Member, IEEE,* and Stefano Trapani

***Abstract*—Even if friction modeling and compensation is a very important issue for manipulators, quite simple models are often adopted in the industrial world to avoid too heavy solutions from the computational point of view, and because of the difficulty of finding and identifying a model applicable in any motion condition. This paper proposes a general framework for friction identification for industrial manipulators with the goal of solving the previous problems through: (i) a complete procedure managing all the steps from data acquisition and model identification up to the generation of the code for the implementation into the robot software architecture, (ii) the possibility of adopting static or dynamic models of different complexity, and (iii) the development of some modifications in the dynamic friction model so to achieve a reliable friction torque estimation at any velocity and acceleration regime, avoiding unfeasible peaks and overestimation. The results of experimental tests carried out for different manipulators prove the validity and generality of the proposed friction model and identification procedure.**

***Index Terms*—Robots, friction, identification.**

I. Introduction

Friction modeling and compensation is a very important issue in industrial robotics, where different motion regimes of the robot joints can be involved in specific applications.

Several friction models are available in literature, with different levels of complexity and ability to capture the various phenomena that can characterize friction. The simplest solutions include only Coulomb and viscous friction, while more complex models (see e.g., [1]–[4]) take into account also stiction and Stribeck effect, and are preferable when both high and low speed motions are involved. In case of very slow motions and velocity reversals, more accurate models are needed, including dynamic friction phenomena, too, like the hysteresis [5], the frictional lag [6], and the varying breakaway force [5], [7]. The choice of the friction model to be adopted must be made taking into account not only the characteristics of the phenomenon, but also the application context and the possible problems and requirements for its identification. For a single manipulator, ad hoc experiments can be carried out to investigate the nature of friction in its joints, and hence choose the *best* model to represent it, to be identified in order to have the *best* reconstruction of the friction torques in the specific velocity regimes in which the manipulator is expected to operate. The situation is quite different in case of several, possibly different manipulators, to be inserted in an industrial context and utilized for various applications, potentially involving very wide velocity regimes. In such a context, additional requirements arise for the friction model to be adopted: (i) it should offer a good trade-off between model accuracy and computational burden; (ii) it should provide a feasible reconstruction of the friction torques in *all* the motion conditions, taking into account that such estimated torques could be employed for different purposes, like compensation and control (as in [8], [9]), but also in the computation of a reliable estimation of the motor currents inside service and diagnostic algorithms (e.g., for collision detection as in [10]–[12], and payload check [13]); (iii) it should be identifiable through some general procedure, suitable for all the manipulators without specific customizations.

Analyzing the current state of the art about friction modeling and identification, and focusing on models including also the dynamic effects, the well-known LuGre model [14], [15] must be surely recalled. Basically, such a model merges a representation of the dynamic effects of friction, assembling the Dahl model in the presliding regime (i.e., using bristles to model the microscopic asperities of the surfaces in contact) with a more complete representation of its behavior in static conditions. The main problems in the LuGre model seem to be relative to the description of the hysteresis behavior. In [16], a different integrated friction model (called the Leuven model) is proposed to improve the presliding behavior, with further modifications in [17] to solve possible discontinuities in the friction force during presliding, and to improve the real-time implementation of the hysteresis force through the adoption of the general Maxwell slip model. Some other approaches, e.g., in [18], introduce elasto-plasticity by using different single state models, which are activated on the basis of a continuous switching function; other models require the introduction of more than one internal state variable, as in [19].

All these accurate dynamic friction models are generally identified and experimentally validated only for specific systems, sometimes having one degree of freedom (dof) only, possibly equipped with high-resolution sensors, and/or applying low velocity motions just to highlight their particular capability in capturing presliding phenomena, as for example in [20], in which a dynamic ElastoPlastic friction model (looking simpler than Maxwell, LuGre and Leuven models) is adopted for a measuring machine in an optical setup, or as in [21], where a friction model-based Frequency Response Analysis (FRA) method is developed for servo systems with phase delays. But only an exhaustive experimental validation carried out

Marina Indri is with the Department of Electronics and Telecommunications, Politecnico di Torino, Corso Duca degli Abruzzi 24, 10129 Torino, Italy, phone: +39 011 0907066, email: marina.indri@polito.it (*Corresponding author*)

Stefano Trapani was with the Department of Control and Computer Engineering, Politecnico di Torino, Torino, Italy; now, he is with COMAU S.p.A., Grugliasco (TO), Italy, email: stefano.trapani@comau.com

for more complex systems (like 6-dof industrial manipulators) in a wide range of motions, possibly with various velocity sign reversals, could definitely clarify if these models could be actually adopted *as they are* in a large-scale industrial context. In such a scenario it is necessary to evaluate (i) if the adopted model is able to provide a feasible reconstruction of the friction torques in all the motion conditions, (ii) if it can actually offer some significant benefit, and (iii) if can be identified avoiding procedures strongly customized for each specific manipulator. The identification procedures proposed in literature are generally applied to simpler friction models only. In [22] a systematic procedure is proposed for the identification of the friction parameters together with the robot's dynamic ones, but only for planar manipulators and adopting a static friction model of polynomial type. In [23] a modular test-bed is proposed for experimental friction identification in modular robot drives of a humanoid robot, but adopting again a static model as in [24], where an improved cuckoo search algorithm is developed. A fast friction estimator based on Lyapunov design method is proposed in [25] in addition to a nonlinear disturbance observer within a complete control scheme for a 6-dof parallel electrical manipulator, but only Coulomb and viscous friction components are taken into account. A similar simple model is adopted in [26], where the identification is performed through the Instrumental Variable (IV) method. Also in [27], where the problem of friction identification is investigated for a 6-dof robot with motion limitations due to the configuration of the environment, the considered friction model includes only a nonlinear viscosity term connected in parallel to a Coulomb friction-spring element.

This work, which benefits from the collaboration of Politecnico di Torino and COMAU S.p.A., has the aim of developing a framework for friction identification in industrial manipulators, having the main characteristics considered as fundamental in the industrial scenario, in order to show that a full, dynamic friction model can be actually applied in such a context, achieving some benefit. The proposed general framework includes: (i) the possibility of adopting static or dynamic friction models, (ii) some modifications in the adopted dynamic model, which is of LuGre type, so to achieve a reliable friction torque estimation at any velocity and acceleration regime, and (iii) general procedures for all the required steps, from data acquisition and parameters identification up to the generation of the code for the introduction of the friction model into the robot software architecture. The choice of a friction model with a structure of LuGre type is motivated by previous research activities, which led to a preliminary version of an identification procedure, developed in [28] considering only the static part of the friction model, and reinforced by the results of the analysis carried out in [29]. Here the authors compare various dry friction models through several numerical tests, showing that the LuGre one is among the ones offering a good trade-off between the ability of well reproducing the main friction effects and the amount of computational burden. It must be stressed that the present work is aimed at obtaining an accurate friction estimation to be used inside the service algorithms based on the usage of a reliable estimation of the motor currents. The proposed procedure is then currently run in parallel to the original COMAU control software, providing the required information to the service algorithms, but it is not used for compensation purposes inside the control scheme yet.

Section II analyzes the characteristics of a dynamic friction model of LuGre type, investigating the problems that may arise in correspondence of velocity sign reversals, both theoretically and experimentally using a COMAU Smart NS12 industrial robot as test-bed. A new function is then proposed to represent the bristles damping, including the dependence on acceleration, too, to solve such problems. Section III illustrates the identification procedure, while the structure of the complete software framework is described in Section IV. The general validity of the friction model and of the identification framework is proven for different robots, i.e., a COMAU Racer3 and a COMAU Racer 7, in Section V. Some issues related to its implementation in the industrial controller of the specific robots or to generic manipulators of different manufacturers, are also discussed. Section VI draws some final conclusions.

II. Friction modeling

Different static friction models including not only Coulomb and viscous components, but also stiction and the Stribeck effect, have been developed and adopted. e.g., as in [1], [3], where the Stribeck effect is represented using an exponential function. In [4], the same behavior is achieved using the arctangent function, so obtaining the following friction model, in which any discontinuity is avoided:

$$\tau_f(v) = \tau_s\, S_0(v) + \tau_{sc}\, \frac{2}{\pi} \arctan(v\,\delta) + \tau_v\, v + \left(\tau_{nlv}\ v^2\right) S_0(v) \tag{1}$$

with

$$S_0(v) = \frac{2}{\pi}\, \arctan(v\, K_v) \tag{2}$$

where v is the motor velocity when the model is used to describe friction on the joint of a robotic manipulator. The coefficients τ_s, τ_{sc}, τ_v and τ_{nlv} are related to the static friction, the difference between Coulomb and static friction, the viscous friction, and the nonlinear viscous friction, respectively. The parameter δ inside the arctangent function defines the shape of the Stribeck effect, whereas $S_0(v)$ provides a continuous approximation of the $sign(v)$ function.

Static friction models, like (1), can be included into LuGre-like dynamic models to take into account also additional friction effects. The LuGre friction model [14], [15] has the following general form:

$$\dot{z} = v - \sigma_0 \frac{|v|}{g(v)} z \tag{3}$$

$$\tau_f = \sigma_0 z + \sigma_1 \dot{z} + \tau_{fv}(v) \tag{4}$$

where $g(v)$ models the Stribeck effect, and $\tau_{fv}(v)$ represents the viscous friction behavior. Friction in the pre-sliding regime is modeled representing the microscopic asperities of the surfaces in contact through bristles, whose average deflection is given by the internal state variable z; σ_0 and σ_1 represent the elastic component and the damping factor of the bristles, respectively.

The friction model adopted in the proposed framework has an overall structure similar to the LuGre one, but with the

following modifications: (i) the static model (1)-(2), developed in [4] and included in the preliminary version of the friction identification framework proposed in [28], is used to avoid the presence of any discontinuous operator in its formulation; (ii) a function f_{σ_1} is adopted to represent the bristle damping, instead of a constant σ_1 parameter, in order to achieve a friction model suitable for very different motion conditions.

The overall expression of the adopted friction model is then given by:

$$\dot{z} = S_0(v)^2 v - \sigma_0 \frac{S_1(v)}{g(v)} z \tag{5}$$

$$\tau_f = \sigma_0 z + f_{\sigma_1}(\cdot)\, \dot{z} + \tau_{fv}(v) \tag{6}$$

with

$$S_1(v) = S_0(v)\, v \tag{7}$$

$$g(v) = \tau_s + \tau_{sc} \frac{2}{\pi} \arctan(S_1(v)\, \delta) \tag{8}$$

$$\tau_{fv}(v) = \tau_v\, v + \left(\tau_{nlv}\, v^2\right) S_0(v) \tag{9}$$

where $S_1(v)$ provides a continuous approximation of the $abs(v)$ function, while the expression of $f_{\sigma_1}(\cdot)$, not provided now, will be discussed and developed in the remaining of the section.

Some researchers already noticed a variability of the bristles damping factor, and included its dependence on velocity through different functions of v. For example, in [30] the following possible expressions were suggested:

$$f_{\sigma_1}(v) = \sigma_1 \frac{g(v)}{|v|} \tag{10}$$

$$f_{\sigma_1}(v) = \frac{\sigma_1}{|v|} \tag{11}$$

whereas in [4] a different solution based on the results of [31] was adopted, given by:

$$f_{\sigma_1}(v) = \sigma_1 \left(1 - \frac{2}{\pi} \arctan(|v|\delta)\right) \tag{12}$$

where the values of $\left(1 - \frac{2}{\pi} \arctan(|v|\delta)\right)$ are between 0 and 1.

The introduction of a proper function to model the bristles damping factor is very important. The adoption at any velocity regime of the constant value of σ_1, identified at low velocity (i.e., in the condition suitable for observing the dynamic behavior of friction) may lead to possible unfeasible effects when the velocity changes rapidly or immediately after its sign reversal. Some simulations have been performed using the friction model (5)-(9), with the parameter values that were identified for the first joint of a COMAU Smart NS 12, here listed in the proper SI units: $\tau_s = 0.4012$, $\tau_{sc} = 6.7333 \cdot 10^{-2}$, $\tau_v = 2.7662 \cdot 10^{-3}$, $\tau_{nlv} = -1.5330 \cdot 10^{-6}$, $\delta = 0.1$, $\sigma_0 = 11.655$, $\sigma_1 = 5.8996$. In particular, the identification procedure developed in [28] was applied to identify the first five parameters, i.e., the ones of the static part of the model. Those of the dynamic part (i.e., σ_0 and σ_1), were determined as in [4] assuming a constant bristles damping factor (i.e., for $f_{\sigma_1}(v) = \sigma_1$), and applying nonlinear identification methods to the samples acquired at very low velocities slowly growing, as in the first 15 seconds of the profile reported in Figure 1. The complete velocity profile shown in this figure has then been applied in simulation to evaluate the friction torque behavior during slow and fast velocity sign reversals, as reconstructed using the different expressions for the bristles damping factor.

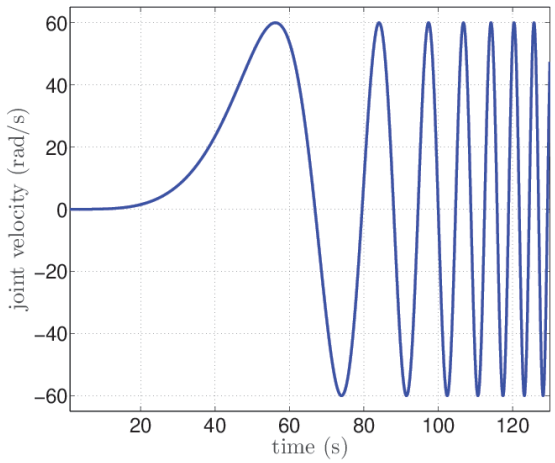

Figure 1: Applied velocity profile; maximum velocity and acceleration are consistent with motor constraints.

Figure 2 shows the results obtained when (*i*) $f_{\sigma_1}(v) = \sigma_1$ (blue solid line), with σ_1 given by the value previously estimated at very low velocity, (*ii*) $f_{\sigma_1}(v)$ is defined as in (11) (black solid line), and (*iii*) when $f_{\sigma_1}(v)$ is as in (12) (magenta dashed line).

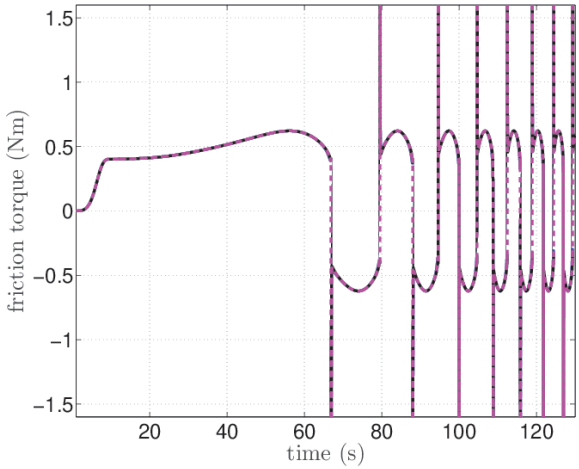

Figure 2: Friction torque estimated with: $f_{\sigma_1} = \sigma_1$ (blue solid line), f_{σ_1} as in (11) (black solid line), f_{σ_1} as in (12) (magenta dashed line).

As the figure clearly shows, in all the cases unfeasible peaks arise in the time history of the reconstructed torque immediately after the velocity sign reversals. A similar simulation test (not reported for space reasons) performed using the expression (10) for $f_{\sigma_1}(v)$ showed the same behavior obtained with (11). The friction peaks are wrongly generated

This article has been accepted for publication in a future issue of this journal, but has not been fully edited. Content may change prior to final publication. Citation information: DOI 10.1109/TMECH.2020.2980435, IEEE/ASME Transactions on Mechatronics

each time the velocity changes its sign very rapidly, i.e., when the applied acceleration is greater than the one adopted during the identification of the dynamic part of the friction model.

A further experimental campaign of tests, carried out imposing to the first joint of the robot a series of motion reversals with different acceleration values, has provided the results reported in Figure 3. A wide range of values has been identified for σ_1 as the acceleration varies, from the initial value of about 5.9 kg m^2/s estimated in the most suitable low velocity conditions for evaluating the dynamic behavior of friction, with an acceleration value of 5.5 rad/s^2, up to 0.004 kg m^2/s or lower for accelerations greater than 500 rad/s^2.

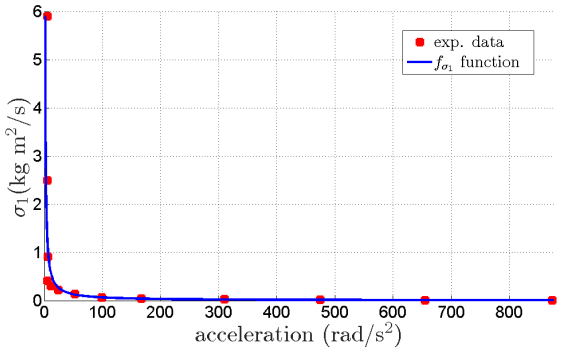

Figure 3: Estimate of the σ_1 parameter for different acceleration values.

On the basis of such results, the adoption of a constant value for σ_1 is not recommended in a friction model that must provide feasible values in a wide range of motion conditions. The expression (12) for $f_{\sigma_1}(v)$, which has provided similar peaks, relies on an implicit strong assumption, given by the usage inside the arctangent function of the same parameter δ that defines the shape of the Stribeck curve in the static part of the friction model. This fact may limit the possibility to adapt $f_{\sigma_1}(v)$ to the actual behavior of the bristles, and hence of the friction torque, when the Stribeck effect is negligible. Our analysis will then focus in the remainder of the section on expression (11) and on possible new solutions for representing the bristles damping.

Figure 4 compares the behavior of the reconstructed friction torque using expression (11) when the maximum identified value for σ_1 (green dashed line) and the minimum one (blue solid line) among the ones reported in Figure 3 are adopted. In the second case the peaks disappear, since the identification performed at very high acceleration values has not allowed to evaluate in practice the contribution of the bristles damping factor, which has been identified as negligible (0.004 kg m^2/s); as a consequence, the friction torque reconstructed in the first seconds of the motion profile is significantly different from the one previously (properly) estimated (green dashed line), as highlighted in the zoom.

Other experimental tests (not reported for space reasons), carried out on different joints/different robots, showed that when the Stribeck effect is more significant, the friction torque reconstruction in the first time instants is even worse, if σ_1 is identified at high acceleration values.

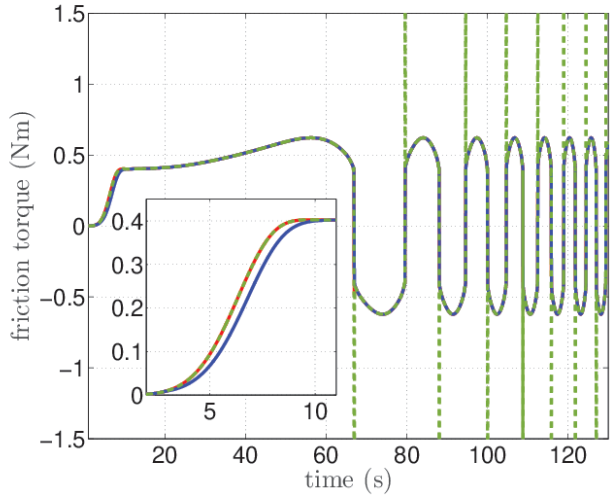

Figure 4: Friction torque estimated with: f_{σ_1} as in (11) with the maximum (green dashed line) and the minimum (blue solid line) identified value of σ_1, and f_{σ_1} as in (24) (red solid line).

Figure 5 shows the time history of the $f_{\sigma_1}(\cdot)\dot{z}$ term in (6) in the considered cases. It is evident that the peaks of the friction torque in Figure 4, when the maximum identified value of σ_1 is adopted in (11), are directly due to the peaks that the term $f_{\sigma_1}(\cdot)\dot{z}$ shows (green dashed line in both figures). The zoom in the lower part of Figure 5 shows in detail what happens after about 67 s, when the first friction peak appears.

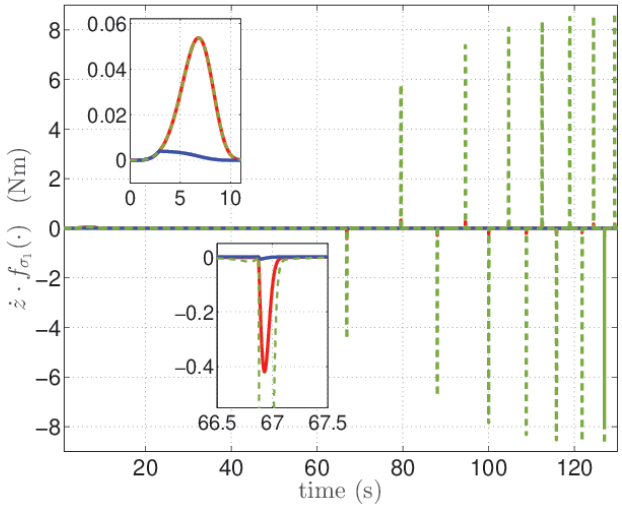

Figure 5: Time history of the $f_{\sigma_1}(\cdot)\dot{z}$ term with: f_{σ_1} as in (11) with the maximum (green dashed line) and the minimum (blue solid line) identified value of σ_1, and f_{σ_1} as in (24) (red solid line).

The adoption of the minimum identified value instead (blue solid line in Figures 4 and 5) corresponds to the absence of any peak in the term, and hence in the reconstructed friction torque. The zoom in the upper part of Figure 5 compares the contribution of this term in the first time instants, highlighting the inability to actually capture the influence of the bristles

damping when the minimum value of σ_1 is considered (blue solid line).

Finally, the red lines in Figures 4 and 5 are relative to the new expression (24) of the bristles damping, which will be proposed and discussed in the last part of this section.

The problems related to the peaks of the $f_{\sigma_1}(\cdot)\dot{z}$ term when the maximum value of σ_1 is adopted, can be analyzed in detail considering $f_{\sigma_1}(\cdot) = f_{\sigma_1}(v) = \sigma_1$ for the sake of simplicity, as in the standard LuGre friction model. In such a case it results:

$$f_{\sigma_1}(\cdot)\dot{z} = \sigma_1\dot{z} = \sigma_1 \cdot v \cdot w(z,v) \tag{13}$$

where the expression of $w(z,v)$ can be determined from the friction model (5)-(9) as:

$$w(z,v) = \left(S_0(v)^2 - \frac{S_0(v)\sigma_0}{g(v)}z\right) \tag{14}$$

Such a function is bounded and converges to zero when $\dot{z} = 0$ (i.e., when z reaches its steady-state value $S_0(v)g(v)/\sigma_0$). During the first part of the transient time of z, function $w(z,v)$ takes values greater than 1, thus increasing the contribution of the $\sigma_1\dot{z}$ term in (6). If the transient time of z is much longer than the time required by the velocity to reach some not negligible value v_m, the term $\sigma_1\dot{z}$ becomes dominant in the computation of τ_f in (6), leading to possible, unfeasible friction peaks. The time t_h required by $w(z,v)$ to become equal to or less than 1 could be exactly computed only by solving the differential equation (5) taking into account the entire velocity profile. A lower limit of t_h can be computed by considering the system response to a velocity step function $v(t) = v_m$, applied starting from a steady state situation (i.e., with $\dot{z} = 0$), with $v(t) = -v_m$ as initial condition, where v_m is a positive not negligible velocity value such that $S_0(v_m) \approx 1$. In such a case (5) becomes a linear differential equation of first order:

$$\dot{z} + \sigma_0\frac{S_0(v_m)v_m}{g(v_m)}z = S_0(v_m)^2 v_m \tag{15}$$

whose solution has the following form:

$$z(t) = e^{-\frac{\sigma_0 S_0(v_m)v_m}{g(v_m)}t}\left(c + \frac{S_0(v_m)g(v_m)}{\sigma_0}e^{\frac{\sigma_0 S_0(v_m)v_m}{g(v_m)}t}\right) \tag{16}$$

Computing c as:

$$c = -2\frac{S_0(v_m)g(v_m)}{\sigma_0} \tag{17}$$

by imposing the initial condition, (16) can be rewritten as:

$$z(t) = \frac{S_0(v_m)g(v_m)}{\sigma_0}\left(1 - 2e^{-\frac{\sigma_0 S_0(v_m)v_m}{g(v_m)}t}\right) \tag{18}$$

Substituting it in (14) for $v(t) = v_m$ it results:

$$w(z,v_m) = 2S_0(v_m)^2 e^{-\frac{\sigma_0 S_0(v_m)v_m}{g(v_m)}t} \tag{19}$$

and hence, since $S_0(v_m) \approx 1$:

$$w(z,v_m) \approx 2e^{-\frac{v_m\sigma_0}{g(v_m)}t} \tag{20}$$

Function $w(z,v_m)$ approximately reaches 1 at

$$t = \frac{\log(2)g(v_m)}{v_m\sigma_0} \tag{21}$$

The actual time t_h taken by $w(z,v)$ to become equal to or less than 1 will be longer, since velocity grows according to the applied velocity profile and reaches the v_m value only after a while; in case of a constant acceleration a_m, such a value would be reached at $t_{vm} = v_m/a_m$, thus implying that for

$$a_m \geq \frac{\sigma_0 v_m^2}{\log(2)g(v_m)} \tag{22}$$

$v(t)$ becomes greater than v_m while $w(z,v)$ is still greater than (or equal to) 1, thus causing the unfeasible estimated friction peaks that occurred in the carried out tests. Since high acceleration values are usually applied to industrial manipulators working in standard conditions, such a critical situation must be considered as common.

According to the experimental results reported in Figure 3, and to the above analysis, the dependence of $f_{\sigma_1}(\cdot)$ on acceleration is then introduced to take into account the influence of the rapidity with which velocity changes its sign. The observed behavior can be easily reproduced using a function inversely proportional to acceleration as:

$$f_{\sigma_1}(a) = \frac{\alpha}{|a|} + \beta \tag{23}$$

where α and β are two parameters to be estimated. In order to avoid possible numerical problems when the system is moving at constant velocity (i.e., when $a \approx 0$), (23) is modified to include the dependence on velocity, too, thus obtaining:

$$f_{\sigma_1}(v,a) = \frac{\alpha}{\sqrt{\gamma\,(\frac{a_{max}}{v_{max}}v)^2 + a^2}} + \beta \tag{24}$$

where a_{max} and v_{max} are the maximum acceleration and velocity values reached by the joint during the data acquisition procedure, respectively. Their ratio a_{max}/v_{max} is used as a normalization coefficient, whereas γ is a weighting coefficient that adapts the behavior of the function in different velocity regimes, to be identified together with α and β. The time-history of the reconstructed friction torque and of the bristles damping term, when the proposed function (24) is adopted, are reported with a red solid line in Figures 4 and 5, respectively, by using the values of α, β and γ estimated by the proposed procedure (illustrated in Section III), providing in particular $\alpha = 6.509$ m^{2}kg/s^3, $\beta = 0$, $\gamma = 1.058$, and $a_{max}/v_{max} = 5.276$ s^{-1}.

As highlighted in the zoom of Figure 4, the ability of capturing the bristles damping action in the first time instants is maintained, while no appreciable peak is present in the rest of the motion. The lower zoom in Figure 5 shows that a very limited peak (about ten times smaller than the one obtained using function (11) with the maximum value of σ_1) is present in the behavior of the damping term. The proposed function (24) then provides a good trade-off to properly reconstruct friction in all the situations, and is then adopted in the dynamic friction model (5)-(9) included in the proposed identification procedure, which is illustrated in the next section.

The usage of acceleration in (24) is not a limitation for the implementation of the proposed model in the software control architecture of industrial manipulators, which are not usually equipped with accelerometers, since acceleration is

used only to properly tune the value of the bristles damping. A low precision can then be acceptable, as well as the use of the reference acceleration values instead, or of the estimates provided by an observer (as in the experimental tests reported in Section V). It must be finally noted that the proposed model does not take into account effects due to temperature [32] or load [33] variations, which could be eventually included in the static part of the model.

III. Identification procedure

The parameters of the complete friction model (5)-(9), (24) are found by means of a two step approach, where Step 1 provides the parameters values of the static model (8)-(9), and Step 2 computes the parameters values of the dynamic part of the model given by equations (5)-(6), and (24).

As already discussed in [28], the friction identification process is carried out using the so-called residual torques, given by the difference between the command torques applied to the joints and those computed by the robot dynamic model (supposed to be available) without the inclusion of any friction term. The friction identification on the i-th joint is then fed by the torque $\tau_{res,i}$, defined as:

$$\tau_{res,i} = \tau_{m,i} - \tau_{dm,i} \tag{25}$$

where $\tau_{m,i}$ represents the command torque applied to the joint (obtained as the product of the motor current and the corresponding motor constant), whereas $\tau_{dm,i}$ is i-th component of the vector $\tau_{\mathbf{dm}}$ defined as:

$$\tau_{\mathbf{dm}} = \mathbf{K_{tr}^{-1}} \cdot \left[\mathbf{M}(\mathbf{q})\ddot{\mathbf{q}} + \mathbf{C}(\mathbf{q}, \dot{\mathbf{q}})\dot{\mathbf{q}} + \mathbf{g}(\mathbf{q})\right] \tag{26}$$

where $\mathbf{q}$ is the joint position vector, $\mathbf{M}(\mathbf{q})$ is the inertial matrix, $\mathbf{C}(\mathbf{q}, \dot{\mathbf{q}})$ is the matrix including centrifugal and Coriolis effects, $\mathbf{g}(\mathbf{q})$ includes the gravity torques; $\mathbf{K_{tr}}$ is a diagonal matrix containing the transmission ratio of each joint.

A. Step 1: Identification of the static friction model

The parameters identification of the static part (8)-(9) of the model is carried out by following the procedure developed in [28], which requires a set of data acquisitions carried out at different velocities, for each joint. The acquisitions are made moving one joint at a time and imposing wide movements with high accelerations, so to maximize the portion of movement carried out at constant velocity. In order to properly model the Stribeck effect, it is recommended to perform a great number of acquisitions at very low velocities, so to have more samples in the initial region of the friction curve modeled as a function of velocity. The parameters identification is based on the solution of a Linear In Parameter problem, once the non linear terms have been fixed. The approach then relies on the a priori definition of the values of K_v and δ, and the computation of the remaining parameters using the Least Square (LS) method as:

$$\theta = \left(\Phi\Phi^T\right)^{-1}\Phi\,\mathbf{T}_f \tag{27}$$

where

$$\Phi = \left[\tfrac{2}{\pi}arctan(\mathbf{v}\,K_v),\ \tfrac{2}{\pi}arctan(\mathbf{v}\,\delta),\ \mathbf{v},\ \mathbf{v}^2\tfrac{2}{\pi}arctan(\mathbf{v}\,K_v)\right]$$
$$\theta = \left[\tau_s,\ \tau_{sc},\ \tau_v,\ \tau_{nlv}\right]^T \tag{28}$$

whereas $\mathbf{T_f}$ and $\mathbf{v}$ are two vectors containing the data samples of $\tau_{res,i}$ and of the velocity, respectively, for the considered joint.

The parameter K_v is used inside the arctangent function to obtain a continuous approximation of the *sign* function; its value is set to 1000 as proposed in [28], as a trade off between the necessity of approximating the *sign* function very well, and the need to avoid discontinuities when the joint velocity goes to zero.

The parameter δ must be properly chosen so that the friction model fits the experimental data, since it defines the shape of the Stribeck effect. Also its computation is performed using the methodology proposed in [28], which is based on a minimum search algorithm testing all the possible values of δ within a feasible set. Such a procedure applies the LS estimation for each value of δ within the set, and computes the error between the experimental data and the values obtained using the model; at the end of the procedure the set of parameters minimizing such an error is selected. This approach is not computationally heavy, since the set of possible values of δ is quite small, and the increment step can be kept high; as in [28], the minimum search algorithm is here applied using values between 0 and 100, with an increment step of 0.1.

At this point the complete vector Θ_{sm} of the parameters of the static friction model, including θ (28) and δ, is available.

B. Step 2: Identification of the dynamic friction model

The identification process of the entire friction model (5)–(9), (24) is here completed. This step is divided into two phases: (i) phase 2-A in which the model (5)-(6) is adopted using a constant σ_1 coefficient instead of the function $f_{\sigma_1}(\cdot)$, in order to estimate the coefficients σ_0 and σ_1 for different datasets, collected at different motion conditions, and (ii) phase 2-B where the values of σ_0 and σ_1 gathered in step 2-A are exploited to compute the parameters of (24) and to definitely set the value of σ_0.

The procedure needs a set of data acquisitions collected for different velocity profiles, each of which is obtained applying a single joint motion, characterized by a continuous cyclical movement between a starting and a final point. Each velocity profile is specifically designed to have a particular acceleration value during the motion reversals. A further data acquisition is carried out, imposing more variability in terms of velocities and accelerations during the joint movements, to collect the experimental data for the identification phase 2-B.

Phase 2-A: The dynamic friction model (5)-(6) integrates the static model (8)-(9), which is completely known after the first identification step described in Section III-A; only σ_0 and σ_1 must be still identified, assuming in this phase that the function f_{σ_1} coincides with a constant σ_1 value. Because of the nonlinear characteristic of the model, a nonlinear identification method must be applied. The adopted identification procedure aims at minimizing a cost function given by the weighted norm of the prediction error, i.e., the difference between the experimental data and the predicted output obtained by the model. The optimization problem is solved using the "System Identification Toolbox" of MATLAB, in which the friction

This article has been accepted for publication in a future issue of this journal, but has not been fully edited. Content may change prior to final publication. Citation information: DOI 10.1109/TMECH.2020.2980435, IEEE/ASME Transactions on Mechatronics

model is specified by means of a first-order nonlinear differential equation using the "Nonlinear Grey-Box Model Structure", whereas the estimation is carried out using the PEM instruction [34]. The output of the identification procedure provides the values of σ_0 and σ_1 that allow to best fit the experimental data.

The identification procedure just illustrated would require only one data acquisition at low velocity, keeping σ_1 constant. Applying such an identification procedure to different data acquisitions, each of which obtained imposing motion reversals to the joint at different acceleration values, it is possible to observe the trend of σ_1, as shown in Figure 3, and to proceed to the identification of the parameters of $f_{\sigma_1}(v, a)$ in (24).

Phase 2-B: The parameters of (24) are estimated using the information provided by steps 1 and 2-A following three sequential steps: (i) identification of α and β, (ii) computation of the ratio a_{max}/v_{max}, and (iii) identification of γ.

Parameters α and β of the basic model (23) are estimated by applying a standard LS approach, using the values of σ_1 identified at different acceleration values as samples of f_{σ_1}. The second step computes the ratio a_{max}/v_{max} from the maximum acceleration and velocity values reached during the motion performed with the highest acceleration. The third step is carried out using the nonlinear identification method adopted in Phase 2-A; this time the complete model (5)-(9), (24) is introduced in the "System Identification Toolbox", where all the model parameters are known except for γ, which is left as free and here estimated.

The procedure ends definitely setting the value of σ_0 equal to the one estimated at the end of Phase 2-A, when the slowest movement was applied (i.e., in the most suitable conditions for evaluating the bristles behavior). All the parameters of the dynamic part of the friction model, σ_0, α, β, γ, and the ratio a_{max}/v_{max} are hence available, and collected in vector Θ_{dm}.

IV. Complete Friction Identification Framework

The framework for friction identification proposed in [28] provides practical information to carry out the data acquisition, the parameter identification and the implementation of the static model (1) only. Different issues are already addressed in [28], like those related to the data pre-processing, (e.g., cleaning and splitting phases), the management of the model validity region and the identification procedure.

The complete framework herein proposed, including the dynamic friction model (5)-(9), (24), and the corresponding identification procedure described in Subsection III-B, is based on a modular approach leaving the user the possibility of identifying the friction static model only, or the complete one. Figure 6 shows the flow-chart of the new complete framework, where the red parts represent the portion of the procedure devoted to the identification of the static model parameters, including the static friction framework developed in [28], whereas the blue ones extend the identification procedure to the complete friction model. The red flow is always executed, since its results are required to estimate both the static model and the complete one, while the blue flow is executed optionally. This way the lighter static model can be identified and used in applications mainly involving medium and high velocities, whereas the complete dynamic one is determined and adopted when necessary for applications requiring slow, precise motions of the robot.

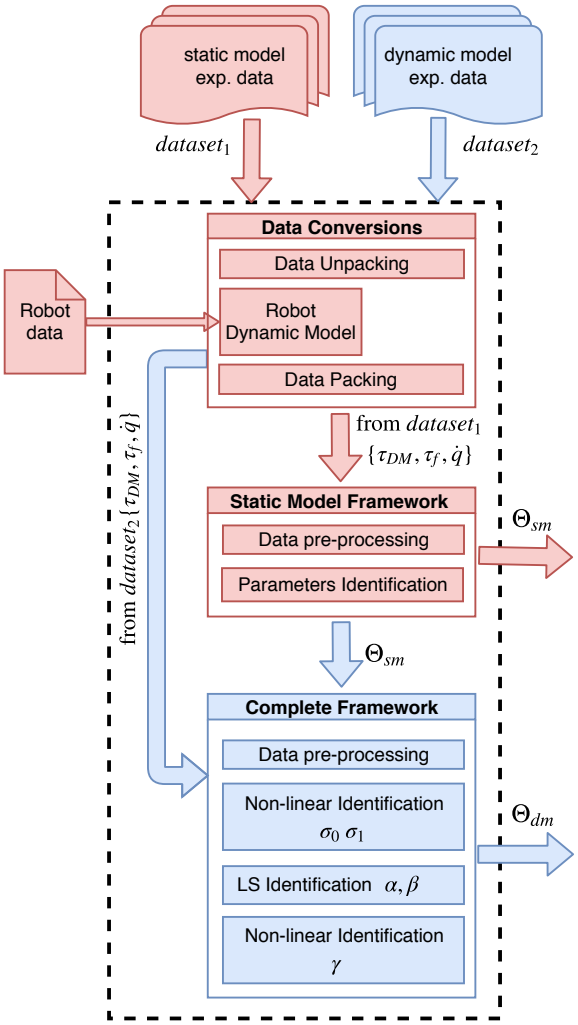

Figure 6: Flowchart of the whole friction identification framework.

A *Data Conversions* block has been included to convert the experimental data from the starting format (depending on the specific robot constructor) into the internal framework format. Such a task is carried out by the *Data Unpacking* and *Data Packing* blocks, respectively, where the first one must be properly defined based on the specific file format. For example, the COMAU data acquisition procedure provides a moni.log file, whose format must be properly taken into account to write the corresponding *Data Unpacking* function.

As explained in Section III, the identification procedure requires the residual torques as input; in the original framework such values were provided by the control unit itself, through a special moni.log file, but in the new framework a specific block, called *Robot Dynamic Model*, has been introduced, which computes the robot dynamic model using the Recursive Newton Euler algorithm, so making the identification procedure more general and efficient. The introduction of this

block obviously requires the complete knowledge of the robot characterization.

When only the identification of the static friction model is required, one set of data acquisitions ($dataset_1$), obtained as described in Subsection III-A, must be available. During the identification procedure, the experimental data are firstly converted using the *Data Conversions* block, and then the *Static Model Framework* described in [28] is applied. In such a phase the framework firstly carries out the data pre-processing, involving the cleaning up of the data, the splitting (if necessary), and the computation of some statistic information, and then performs the identification phase, providing the vector of parameters Θ_{sm}, as described in Subsection III-A.

If the parameters of the complete dynamic model are required instead, the procedure continues using a further set of data acquisitions ($dataset_2$), obtained as reported in Subsection III-B. The *Complete Framework* block takes both vector Θ_{sm} and the experimental data properly elaborated by the *Data Conversions* block (which in this case operates on both the data sets), and starts the pre-processing phase aimed at removing possible high frequency sensor noises, through a proper filtering action. The three identification steps described in Subsection III-B are then carried out, so providing vectors Θ_{sm} and Θ_{dm} containing the parameters of the complete friction model.

The proposed framework has been designed to be as general as possible, and to be easily applicable to different robot manufacturers; the parts of the framework actually dependent on the specific robot producer and on the particular adopted robot, have been gathered in the *Data Conversions* block. Two actions are then required to prepare the framework to work with data-sets provided by a specific robot controller: (i) writing a *Data Unpacking* routine that extracts the data from the data acquisition file, and (ii) providing the robot characterization to the *Robot Dynamic Model* block.

For the experimental tests reported in Section V, two different COMAU robots are used in addition to the NS 12, each of which is managed by the C5G COMAU controller. The ongoing collaboration between COMAU and Politecnico di Torino has allowed to simplify the definition of the *Data Unpacking* block, thanks to the complete knowledge of the moni.log file format, as well as to obtain the full description of the considered robots. Some guidelines for the implementation into an OPEN architecture are provided at the end of the next section.

V. Experimental tests

The first set of tests, in which the COMAU NS12 robot is used again, is aimed at proving the validity of the proposed friction model, while the general validity of the identification framework is checked applying it to different robots in the subsequent sets of tests.

The results of the tests are processed inside a Simulink project allowing to compare the torques actually applied by each motor with the ones computed using different friction models. The real torques are obtained transforming the motor currents (included in the moni.log file) into the corresponding torques by means of the motor constant, whereas the estimated torques are computed by summing the contribution of the friction model to that provided by the *Robot Dynamic Model* block, included in the Simulink project. The first tests aim at evaluating the performance of the proposed complete model (denoted as DM2 in the Tables of the results) and comparing it with the purely static friction model (1) (denoted as SM), and the complete friction model (5)-(9) with the f_{σ_1} function given in (11) (denoted as DM1). The tests are performed using only the first joint of the COMAU robot NS 12 - 1.3 in order to neglect the gravity effects, through three specific motion programs. All the programs apply a continuous joint movement in a wide range of positions. The first one uses a random variation of the maximum velocity in the range 1.5 rad/s – 220 rad/s and accelerations between 28 rad/s^2 and 1080 rad/s^2 to test the models in different motion conditions; the second one is relative to medium velocity conditions in the range $5-80$ rad/s, with acceleration range $1.5-147.4$ rad/s^2, whereas the third one includes only low velocities, with peaks not higher than 0.5 rad/s and accelerations between 1.3 rad/s^2 and 8.2 rad/s^2, so to highlight the improvements achieved by the proposed dynamic friction model in the theoretically most favorable conditions.

For each test the following Performance Indices (PI) are computed and reported in Table I: the Root Mean Square (RMS), the Mean (M), and the Infinite Norm (IN) of $\tau_{diff} = \tau_{res} - \tau_f$, with the friction torque τ_f estimated by the three considered models. The performance indices of the proposed model DM2 are then compared to the other ones by computing the relative percentage error ($Err\%$).

Tests	PI	DM2	DM1	SM	$Err\%$ DM1	$Err\%$ SM
Random velocity	RMS	0.0889	0.0904	0.0918	-1.7	-3.3
	M	0.0624	0.0632	0.0636	-1.3	-2
	IN	0.5735	0.6823	0.6627	-19	-15.5
Medium velocity	RMS	0.0760	0.0785	0.0846	-3.2	-11.4
	M	0.06	0.062	0.0645	-3.2	-7.4
	IN	0.4042	0.4795	0.7012	-18.6	-73.5
Low velocity	RMS	0.08	0.1186	0.2077	-48.3	-159.7
	M	0.0683	0.0939	0.1797	-37.5	-163.3
	IN	0.2370	0.2814	0.3993	-18.7	-68.5

Table I: Performance Indices for the first joint of a COMAU NS12.

Table I shows that the new model provides good results in all the motion conditions, since when a random velocity is applied all the performance indices show some improvement, even if small; the most significant improvement is relative to the IN index, i.e., to the maximum error in friction estimation. As velocity decreases in the other two tests all the PIs improve, giving the best results when the velocity is very low.

The second group of tests aims at evaluating the applicability of the framework in general, and the validity of the proposed modified friction model, by applying the complete friction framework illustrated in Section IV to different robots made available by COMAU, with no modification apart from the robot characterization adopted in the *Robot Dynamic Model* block. A first test is performed using a Racer 3 robot and imposing to it a Cartesian trajectory requiring the motion

This article has been accepted for publication in a future issue of this journal, but has not been fully edited. Content may change prior to final publication. Citation information: DOI 10.1109/TMECH.2020.2980435, IEEE/ASME Transactions on Mechatronics

of all the joints. The goal of such a test is to compare the performances of the proposed model with those of the ones often adopted in industrial context (usually static friction models), in order to evaluate them in a generic motion condition. In particular, the test includes a set of Cartesian linear movements, corresponding to a cube shaped path, carried out at a quite low Cartesian velocity (about 250 mm/s), in which all the joints simultaneously move in rather variable motion conditions. The performances of the proposed complete DM2 model, the static SM model, and the one already included inside the COMAU controller (denoted by CM) are compared. Such an internal COMAU model includes only the Coulomb term and the viscous one, with a proper management of motion reversals (whose details are not available) to avoid discontinuities. The DM1 model is not included in such a test, since it will be evaluated in the following one. The results of the test are summarized in Table II, where the performance indices and the corresponding relative percentage errors are reported for all the axes of the COMAU Racer 3.

Tests	PI	DM2	SM	CM	$Err\%$ SM	$Err\%$ CM
Axis 1	RMS	0.0603	0.1063	0.1260	-76.4	-109.1
	M	0.0474	0.0735	0.1054	-55	-122.3
	IN	0.4172	0.4789	0.4342	-14.8	-4.1
Axis 2	RMS	0.0479	0.0498	0.0757	-3.9	-58
	M	0.0313	0.0335	0.0629	-6.8	-100.5
	IN	0.4953	0.4953	0.5433	-0.0	-9.7
Axis 3	RMS	0.035	0.0335	0.0401	4.3	-14.6
	M	0.0226	0.0212	0.0277	6	-22.7
	IN	0.3756	0.3756	0.3583	0.0	4.6
Axis 4	RMS	0.017	0.0202	0.0291	-19.4	-71.9
	M	0.0121	0.0138	0.0233	-14	-92.2
	IN	0.1396	0.1384	0.1714	1	-22.8
Axis 5	RMS	0.0165	0.0175	0.0185	-6.2	-12.5
	M	0.01257	0.0133	0.0142	-6	-12.7
	IN	0.1629	0.1656	0.1623	-1.7	0.3
Axis 6	RMS	0.0133	0.0219	0.0251	-64.1	-88.3
	M	0.00835	0.0134	0.0199	-61	-138.0
	IN	0.1355	0.1905	0.1678	-40.6	-23.8

Table II: Performance Indices for a COMAU Racer 3 for a cube shaped Cartesian path.

The proposed friction model provides better results also in this case: for all the joints the considered PIs improve, except for some cases in which they remain almost the same, with just few perceptual points of difference. The best results are obtained for axis 6, with a reduction of 138% of the average error between the real joint torques and the ones computed using the robot dynamic model. Slightly worse results are achieved for axis 3, for which the performances obtained using the static model have not been improved by the proposed one. The reasons can be related to the characteristics of the motion of this joint, which is the one reaching the highest velocity in the carried out test. Such a joint is the one that less can benefit from the adoption of the proposed model, which improves the friction representation at low velocities. The small worsening of the IN index with respect to the CM model can be justified by the fact that the CM model has been specifically optimized by COMAU for high velocities, which are of main interest in several applications, at the price of a poor (or very poor) friction estimation at low velocities, as it occurs for example for axes 1 and 6. In particular, analyzing the maximum velocity values reached by each axis during the motion cycle ($\dot{q}_1 = 64$ rad/s, $\dot{q}_2 = 85$ rad/s, $\dot{q}_3 = 124$ rad/s, $\dot{q}_4 = 98$ rad/s, $\dot{q}_5 = 50$ rad/s, $\dot{q}_6 = 68$ rad/s), it can be noticed that axis 3 reaches about twice the velocity of axes 1 and 6, for which the best results are achieved by the proposed model. It is worth to be noticed that the weight of the friction torque with respect to the inertia components varies quite a lot in the different motion phases and for the various axes. The values of R_τ, defined as the ratio between the friction torque and the total torque, corresponding to the current absorbed by the motor, vary on average from 0.40 in the high acceleration phases up to more than 0.90 in the low acceleration phases (i.e., when velocity is constant or almost constant), in which the inertia terms are less significant. This variation range must be considered as an average among all the axes, since some of them may show "extreme" situations. For example, axis 5 is quite light, so that the friction torque is dominant in any motion condition, with R_τ varying between 0.873 (for high accelerations) and 0.997 (for low accelerations).

The final experimental campaign has been carried out considering a COMAU Racer 7 manipulator in addition to the Racer 3. The goal of such tests is to compare the performances of the proposed DM2 model and those of the standard DM1 model for the two robots to verify the general validity of both the model and the framework. The tests performed for the first joint of the NS12 robot have been repeated for all the joints of the Racer 3 and the Racer 7. Figures 7 and 8 show the results related to the IN performance indicator for low and medium velocity, in order to highlight the effects due to the friction peaks at increasing velocity. The figures show

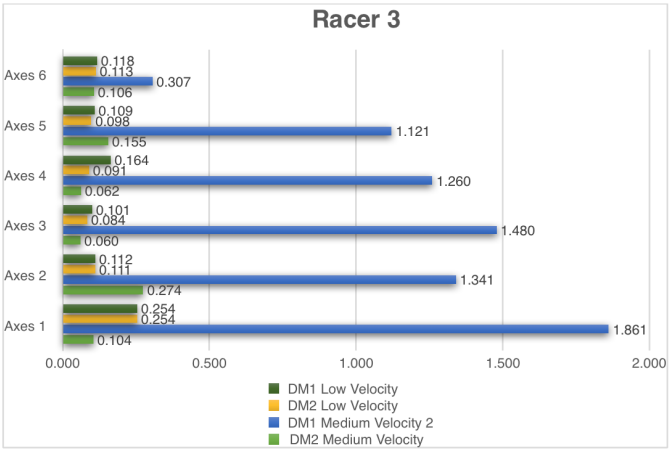

Figure 7: Comparison between friction models DM1 and DM2 using the performance indicator IN obtained at two different velocity ranges (low and medium) for a COMAU Racer 3.

that the infinite norm of the model error dramatically worsens at medium velocity when the DM1 model is used, while it provides better results for low velocity. Such a result is due to the friction peaks introduced by the DM1 model for increasing velocity. The (very) bad results obtained by the application of such a model at medium velocities justify the fact that dynamic friction models are rarely used in the industrial world,

This article has been accepted for publication in a future issue of this journal, but has not been fully edited. Content may change prior to final publication. Citation information: DOI 10.1109/TMECH.2020.2980435, IEEE/ASME Transactions on Mechatronics

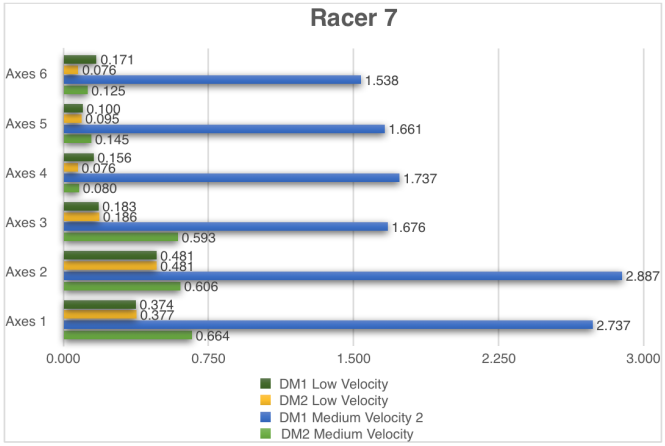

Figure 8: Comparison between friction models DM1 and DM2 using the performance indicator IN obtained at two different velocity ranges (low and medium) for a COMAU Racer 7.

since they seem to introduce problems instead of improving performances. On the contrary, the proposed DM2 model is successfully applied in both the motion conditions to both robots. Figure 9 shows the percentage of reduction of the average model error (performance indicator M) in all the motion conditions (i.e., at low, medium and high velocities), provided by DM2 with respect to DM1 for the Racer 3 and Racer 7 robots. The figure highlights that the improvement is appreciable for all the axes of the robots, although with different percentage values.

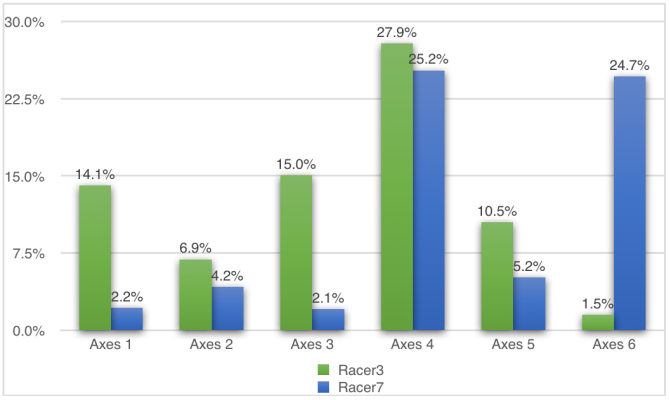

Figure 9: Percentage of reduction of the average model error (indicator M) provided by DM2 with respect to DM1 for Racer 3 and Racer 7 robots.

A. Implementation in a real scenario

The direct implementation of the model in an industrial controller or in a different target hardware has been tested, so to verify the proper functioning of the proposed framework in a real scenario. The complete model (5)-(9), (24) has been discretized in order to be included in the real time system, as:

$$\begin{cases} z_{k+1} = e^{-a_k T_s} z_k + \frac{(1-e^{-a_k T_s})}{a_k} b_k & \text{for } a_k \neq 0 \\ z_{k+1} = z_k + b_k T_s & \text{for } a_k = 0 \end{cases} \quad (29)$$

where T_s is the sampling time, and

$$a_k = \sigma_0 \frac{S_1(v_k)}{g(v_k)}, \quad b_k = S_0(v_k)^2 v_k \quad (30)$$

Two target hardware solutions have been tested: (i) the industrial COMAU controller C5G, and (ii) the OPEN control architecture for the C5G robot controllers. The direct implementation of (29) in the C5G control unit has been made possible by the collaboration between COMAU and Politecnico di Torino. For the second test, carried out using the OPEN control architecture, the discretized model (29) was included into a Simulink project, and the source files were automatically generated using the Simulink "Embedded Code Generation" tool. Figure 10 highlights how the friction framework has been included in the overall work flow that allows to estimate the friction model parameters and to generate the corresponding C/C++ code.

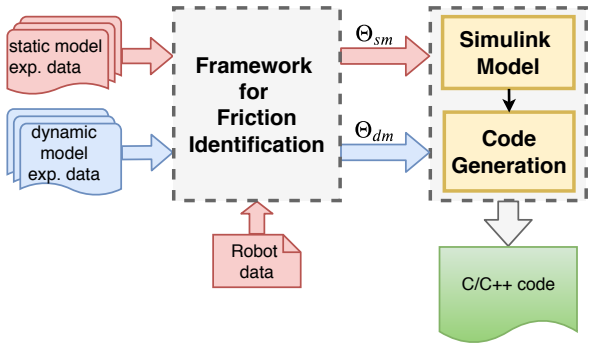

Figure 10: Work flow defining the friction identification phase and the code generation one.

The source files were then properly included in the open-source control architecture, to compute the complete robot dynamic model by summing the friction values estimated by the proposed framework and the non-friction terms of the internal robot dynamic model, made available by a basic functionality included in the OPEN architecture. Both the target hardware solutions were tested using the same test programs adopted for the simulations; the same friction behavior was obtained in all the cases. These tests are fundamental for a real, practical implementation of the proposed friction identification framework, since they allow to evaluate the correct working of the complete flow of the procedure, starting from data acquisition up to parameter identification.

VI. Conclusion

The paper proposed a framework for robots friction identification suitable for the industrial context. A scalable friction model given by the composition of a static part and a dynamic one was adopted, to allow the best choice for the target application and the available hardware. The modification introduced in the friction model allowed to successfully apply the new complete model in very different motion conditions, avoiding unfeasible peaks in the friction torque reconstruction. The proposed friction identification framework was applied to different robots of the same manufacturer (i.e., COMAU) but the framework can be implemented also in an OPEN

control architecture, and hence it is potentially available for any generic industrial robot.

REFERENCES

[1] B. Armstrong, "Friction: Experimental determination, modeling and compensation," in *Proc. IEEE Int. Conf. Robot. Autom.*, 1988, pp. 1422–1427.

[2] B. Armstrong-Helouvry, P. Dupont, and C. Canudas De Wit, "A survey of models, analysis tools and compensation methods for the control of machines with friction," *Automatica*, vol. 30, no. 7, pp. 1083–1138, 1994.

[3] C. Canudas de Wit, P. Noel, A. Aubin, and B. Brogliato, "Adaptive friction compensation in robot manipulators: Low velocities," *The Int. J. Robot. Res.*, vol. 10, no. 3, pp. 189–199, 1991.

[4] M. Indri, I. Lazzero, A. Antoniazza, and A. M. Bottero, "Friction modeling and identification for industrial manipulators," in *Proc. IEEE Int. Conf. Emerg. Techn. Factory Autom.*, 2013, pp. 1–8.

[5] V. Lampaert, F. Al-Bender, and J. Swevers, "Experimental characterization of dry friction at low velocities on a developed tribometer setup for macroscopic measurements," *Tribology Letters*, vol. 16, no. 1, pp. 95–105, 2004.

[6] B. Armstrong-Helouvry, "Frictional lag and stick-slip," in *Proc. IEEE Int. Conf. Robot. Autom.*, 1992, pp. 1448–1453.

[7] M. Ruderman, "On break-away forces in actuated motion systems with nonlinear friction," *Mechatronics*, vol. 44, pp. 1–5, 2017.

[8] F. Al-Bender, V. Lampaert, and J. Swevers, "The generalized Maxwell-slip model: a novel model for friction simulation and compensation," *IEEE Trans. Autom. Control*, vol. 50, no. 11, pp. 1883–1887, 2005.

[9] Z. Jamaludin, H. V. Brussel, G. Pipeleers, and J. Swevers, "Accurate motion control of xy high-speed linear drives using friction model feedforward and cutting forces estimation," *CIRP Annals*, vol. 57, no. 1, pp. 403–406, 2008.

[10] A. De Luca and R. Mattone, "Sensorless robot collision detection and hybrid force/motion control," in *Proc. IEEE Int. Conf. Robot. Autom.*, 2005, pp. 999–1004.

[11] M. Indri, S. Trapani, and I. Lazzero, "A general procedure for collision detection between an industrial robot and the environment," in *Proc. IEEE Int. Conf. Emerg. Techn. Factory Autom.*, 2015, pp. 1–8.

[12] ——, "Development of a virtual collision sensor for industrial robots," *Sensors*, vol. 17, no. 5, p. 1148, 2017.

[13] M. Indri and S. Trapani, "Using virtual sensors in industrial manipulators for service algorithms like payload checking," in *Int. Conf. on Robotics in Alpe-Adria Danube Region*, 2017, pp. 138–146.

[14] C. Canudas De Wit, H. Olsson, K. J. Astrom, and P. Lischinsky, "A new model for control of systems with friction," *IEEE Trans. on Autom. Control*, vol. 40, no. 3, pp. 419–425, 1995.

[15] K. Johanastrom and C. Canudas-De-Wit, "Revisiting the lugre friction model," *IEEE Control Systems*, vol. 28, no. 6, pp. 101–114, 2008.

[16] J. Swevers, F. Al-Bender, C. G. Ganseman, and T. Projogo, "An integrated friction model structure with improved presliding behavior for accurate friction compensation," *IEEE Trans. Autom. Control*, vol. 45, no. 4, pp. 675–686, 2000.

[17] V. Lampaert, J. Swevers, and F. Al-Bender, "Modification of the leuven integrated friction model structure," *IEEE Trans. Autom. Control*, vol. 47, no. 4, pp. 683–687, 2002.

[18] P. Dupont, V. Hayward, B. Armstrong, and F. Altpeter, "Single state elastoplastic friction models," *IEEE Trans. Autom. Control*, vol. 47, no. 5, pp. 787–792, 2002.

[19] M. Ruderman and T. Bertram, "Two-state dynamic friction model with elasto-plasticity," *Mech. Syst. Sign. Proc.*, vol. 39, no. 1, pp. 316–332, 2013.

[20] A. Keck, J. Zimmermann, and O. Sawodny, "Friction parameter identification and compensation using the elastoplastic friction model," *Mechatronics*, vol. 47, pp. 168 – 182, 2017.

[21] Y. Maeda, K. Harata, and M. Iwasaki, "A friction model-based frequency response analysis for frictional servo systems," *IEEE Trans. Ind. Inf.*, vol. 14, no. 11, pp. 5146–5155, 2018.

[22] M. Afrough and A. A. Hanieh, "Identification of dynamic parameters and friction coefficients," *J. Intell. Robot. Syst.*, vol. 94, pp. 3–13, 2019.

[23] J. Baur, S. Dendorfer, J. Pfaff, C. Christoph Schutz, T. Buschmann, and H. Ulbrich, "Experimental friction identification in robot drives," in *Proc. IEEE Int. Conf. Robot. Autom.*, 2014, pp. 6006–6011.

[24] L. Ding, X. Li, Q. Li, and Y. Chao, "Nonlinear friction and dynamical identification for a robot manipulator with improved cuckoo search algorithm," *Journal of Robotics*, vol. 2018, Article ID 8219123, 2018.

[25] R. Hao, J. Wang, J. Zhao, and S. Wang, "Observer-based robust control of 6-dof parallel electrical manipulator with fast friction estimation," *IEEE Trans. Autom. Science Eng.*, vol. 13, no. 3, pp. 1399–1408, 2016.

[26] A. Janot, P. Vandanjon, and M. Gautier, "A generic instrumental variable approach for industrial robot identification," *IEEE Trans. Control Syst. Techn.*, vol. 22, no. 1, pp. 132–145, 2014.

[27] M. Iwatani and R. Kikuuwe, "An identification procedure for rate-dependency of friction in robotic joints with limited motion ranges," *Mechatronics*, vol. 36, pp. 36 – 44, 2016.

[28] M. Indri, S. Trapani, and I. Lazzero, "Development of a general friction identification framework for industrial manipulators," in *Proc. IEEE IECON 2016*, pp. 6859–6866.

[29] E. Pennestrì, V. Rossi, P. Salvini, and P. P. Valentini, "Review and comparison of dry friction force models," *Nonlinear Dynamics*, vol. 83, no. 4, pp. 1785–1801, 2016.

[30] H. Olsson, "Control systems with friction," *PhD Thesis*, 1996.

[31] G. Ferretti, G. Magnani, and P. Rocco, "Single and multistate integral friction models," *IEEE Trans. Aut. Control*, vol. 49, no. 12, pp. 2292–2297, 2004.

[32] L. Simoni, M. Beschi, G. Legnani, and A. Visioli, "Modelling the temperature in joint friction of industrial manipulators," *Robotica*, vol. 37, no. 5, pp. 906–927, 2019.

[33] A. C. Bittencourt, E. Wernholt, S. Sander-Tavallaey, and T. Brogårdh, "An extended friction model to capture load and temperature effects in robot joints," in *Proc. IEEE/RSJ Int. Conf. Intell. Robots Syst.*, 2010, pp. 6161–6167.

[34] L. Ljung, "System identification," in *Signal analysis and prediction*. Springer, 1998, pp. 163–173.

Marina Indri received the M.Sc. degree in Electronic Engineering in 1991 and the Ph.D. in Control and Computer Engineering in 1995, both from Politecnico di Torino, Italy. She is currently Associate Professor at the Department of Electronics and Telecommunications of Politecnico di Torino, teaching Robotics and Automatic Control.

She coauthored about 100 papers in international journals, books and conference proceedings, in the fields of robotics and automatic control. Her current research interests are in the industrial and mobile robotics areas. She participated in various research projects and joint activities with industrial partners. She received the best paper award in Factory Automation at IEEE ETFA 2013, the 2nd prize of the euRobotics Technology Transfer Award in 2014 and was among the finalists of the same Award in 2017 for joint works with COMAU S.p.A.

Stefano Trapani was born in 1986 and received the B.Sc. and the M. Sc. degree in Computer Engineering in 2012 and 2014, respectively, both from Politecnico di Torino. Between 2014 and 2015 he was a research assistant at the Department of Control and Computer Engineering of Politecnico di Torino, working on collision detection systems for industrial manipulators and on friction modeling and compensation. In 2015-2019 he carried out his research activity as a PhD student at Politecnico di Torino within a PhD Project in Apprenticeship in collaboration with COMAU, co-funded by Regione Piemonte. His research activity aimed at defining a task based programming of industrial robotic cells. He is currently employed as software developer for the motion group of COMAU robotics.